

Roberge-Weiss endpoint at the physical point of $N_f = 2 + 1$ QCD

Claudio Bonati,^{*} Massimo D'Elia,[†] Marco Mariti,[‡] Michele Mesiti,[§] and Francesco Negro[¶]
Dipartimento di Fisica dell'Università di Pisa and INFN - Sezione di Pisa,
Largo Pontecorvo 3, I-56127 Pisa, Italy

Francesco Sanfilippo^{**}

School of Physics and Astronomy, University of Southampton, SO17 1BJ Southampton, United Kingdom
(Dated: April 13, 2016)

We study the phase diagram of $N_f = 2 + 1$ QCD in the $T - \mu_B$ plane and investigate the critical point corresponding to the onset of the Roberge-Weiss transition, which is found for imaginary values of μ_B . We make use of stout improved staggered fermions and of the tree level Symanzik gauge action, and explore four different sets of lattice spacings, corresponding to $N_t = 4, 6, 8, 10$, and different spatial sizes, in order to assess the universality class of the critical point. The continuum extrapolated value of the endpoint temperature is found to be $T_{RW} = 208(5)$ MeV, i.e. $T_{RW}/T_c \sim 1.34(7)$, where T_c is the chiral pseudocritical temperature at zero chemical potential, while our finite size scaling analysis, performed on $N_t = 4$ and $N_t = 6$ lattices, provides evidence for a critical point in the $3d$ Ising universality class.

PACS numbers: 12.38.Aw, 11.15.Ha, 12.38.Gc, 12.38.Mh

I. INTRODUCTION

The remarkable changes expected for the properties of strongly interacting matter when it is put under extreme conditions are the subject of intense ongoing theoretical and experimental research. Various parameters of phenomenological interest enter the description of such extreme conditions, like temperature, chemical potentials or external background fields. Part of this research consists in the study of the QCD phase diagram, i.e. in mapping the various phases of strongly interacting matter in equilibrium conditions, and the associated phase transitions and critical points, as a function of those parameters.

At high temperature confinement and chiral symmetry breaking are expected to disappear, and QCD is expected to be described in terms of quark and gluon effective degrees of freedom (Quark-Gluon Plasma). Lattice QCD simulations show that, indeed, a rapid change of properties takes place around a well defined temperature T_c . There is no compelling reason for expecting a true phase transition, since no exact symmetry of QCD, which could possibly change its realization at T_c , is known: chiral symmetry is exact only for vanishing quark masses, while the Z_3 center symmetry is exact only in the pure gauge theory, where its spontaneous breaking is associated to deconfinement. In fact, lattice simulations have shown that only a smooth crossover is present in the case of physical quark masses, at a temperature $T_c \sim 155$

MeV [1–5].

The situation could be different in the presence of other external parameters. In particular, the crossover could turn into a real transition for large enough baryon chemical potential μ_B , starting from a critical endpoint in the $T - \mu_B$ plane. Such a critical point, and the associated critical behavior around it, could have a huge impact on strong interactions phenomenology, so that large theoretical and experimental efforts are being dedicated to prove its existence and locate it. Unfortunately, numerical progress by lattice QCD simulations is strongly hindered by the sign problem affecting the path integral formulation at non-zero baryon chemical potential.

There are, however, well defined locations, in an extended QCD phase diagram, where exact symmetries are known for any value of the quark masses. Critical points associated with their spontaneous symmetry breaking are predicted to exist and can be investigated by standard lattice simulations. This is the case of QCD with a purely imaginary baryon chemical potential [6–9], the partition function of which is

$$Z(T, \theta_B) = \text{Tr} \left(e^{-\frac{H}{T}} e^{i\theta_B B} \right) \quad (1)$$

where H is the QCD Hamiltonian, B is the baryon charge and $\theta_B = \text{Im}(\mu_B)/T$. All physical states of the theory, over which the trace is taken, are globally color neutral and carry an integer valued baryon charge B , hence Z is 2π -periodic in θ_B , or alternatively $2\pi/N_c$ -periodic in $\theta_q = \text{Im}(\mu_q)/T$, where $\mu_q = \mu_B/N_c$ is the quark chemical potential and N_c is the number of colors. That can also be proven by making use of center transformations in the path-integral formulation of the partition function, as we review in Section II.

On the other hand, in the high- T phase, quarks, which carry a baryon charge $1/N_c$, become the effective degrees of freedom propagating through the thermal medium: modes which are 2π -periodic in θ_q , hence $2\pi N_c$ periodic

^{*}Electronic address: claudio.bonati@df.unipi.it

[†]Electronic address: massimo.delia@unipi.it

[‡]Electronic address: mariti@df.unipi.it

[§]Electronic address: mesiti@pi.infn.it

[¶]Electronic address: fnegro@pi.infn.it

^{**}Electronic address: f.sanfilippo@soton.ac.uk

in θ_B , appear in the functional dependence of the partition function. As a consequence, the 2π periodicity in θ_B is possible only through the appearance of a non-analytic behavior in $Z(T, \theta_B)$, associated with first order phase transition lines present for $\theta_B = \pi$ or odd multiples of it, which are known as Roberge-Weiss (RW) transitions [10] and have been widely studied by lattice QCD simulations [8, 9, 11–25].

In correspondence with such points, analogously to what happens when θ_B is a multiple of 2π , the theory is invariant under charge conjugation, but contrary to that case charge conjugation is spontaneously broken at high T , where the system develops a non-zero expectation value for the imaginary part of the baryon number density: the temperature T_{RW} where the spontaneous breaking takes place is precisely the endpoint of the Roberge-Weiss first order transition lines. An alternative point of view about the same transition is to look at it as a quantum (i.e. zero temperature) transition, with an associated spontaneous breaking of charge conjugation, driven by the compactification of one of the spatial directions beyond a critical size $L_C = 1/T_{\text{RW}}$ (finite size transition [26, 27]). Since charge conjugation is a Z_2 symmetry, one expects a $3d$ -Ising universality class if the transition is second order, or alternatively a first order transition with the development of a latent heat.

The temperature T_{RW} and the critical behavior to which it is related represent universal properties of strong interactions, directly related to the change in the effective degrees of freedom propagating in the thermal medium, hence to deconfinement. They can be carefully studied by lattice QCD simulations, since the path integral measure is real and positive for imaginary chemical potentials. Despite being related to a critical point located in an unphysical region of the QCD phase diagram, their importance and relevance to a full understanding of strong interactions stems from various considerations:

i) The RW endpoint may influence physics in a critical region around it. Moreover, if at the RW endpoint a first order transition is present, the endpoint is actually a triple point, with further departing first order lines, the endpoints of which may be even closer to the $\mu_B = 0$ axis, with more interesting consequences.

ii) Early studies have shown that the RW endpoint transition is first order for small quark masses, second order for intermediate masses, and again first order for large masses; the three regions are separated by two tricritical points [13–15]. The emergence of this interesting structure has induced many further studies in effective models [28–40] which try to reproduce the essential features of QCD. Moreover, interesting proposals have been made on the connection of this phase structure with that present at $\mu_B = 0$ (the so-called Columbia plot) and on the possibility to exploit the whole phase structure at imaginary chemical potential in order to clarify currently open issues on the phase structure at $\mu_B = 0$, like the order of the chiral transition for $N_f = 2$ [21, 24].

iii) Once the RW endpoint has been precisely located,

it can be taken as a test ground to compare the lattice techniques presently used to locate the critical point at real μ_B , so as to assess their reliability and guide future research on the subject.

iv) The relation of the RW endpoint to the other symmetries of QCD, which are present at least in well defined limits of strong interactions, is an interesting issue by itself, which can help elucidate some fundamental non-perturbative properties of the theory.

In this paper we study the properties of the RW endpoint by lattice simulations of QCD with physical quark masses. Its location T_{RW} is determined for various lattice spacings, corresponding to temporal extensions $N_t = 4, 6, 8, 10$, and then extrapolated to the continuum limit. Moreover we are able to determine its universality class, through a finite size scaling analysis, at two different lattice spacings, namely $N_t = 4, 6$. Finally, in order to approach the issue of the interconnection between chiral symmetry and the RW endpoint, we consider the relation of the endpoint location to the analytic continuation of the pseudocritical chiral transition temperature $T_c(\mu_B)$ to imaginary chemical potentials.

The paper is organized as follows. In Section II we review the general framework regarding the RW endpoint in a path-integral approach and present details about our numerical setup and the observables used to investigate the critical behavior. In Section III we report on our numerical results regarding the universality class of the endpoint, the continuum extrapolated value of T_{RW} and its relation with $T_c(\mu_B)$. Finally, in Section IV we draw our conclusions.

II. GENERAL FRAMEWORK AND NUMERICAL SETUP

We consider a staggered discretization of the $N_f = 2+1$ QCD partition function in the presence of imaginary quark chemical potentials:

$$\begin{aligned}
 Z &= \int \mathcal{D}U e^{-S_{YM}} \prod_{f=u,d,s} \det \left(M_{\text{st}}^f[U, \mu_f, I] \right)^{1/4}, \quad (2) \\
 S_{YM} &= -\frac{\beta}{3} \sum_{i, \mu \neq \nu} \left(\frac{5}{6} W_{i; \mu\nu}^{1 \times 1} - \frac{1}{12} W_{i; \mu\nu}^{1 \times 2} \right), \quad (3) \\
 (M_{\text{st}}^f)_{i,j} &= am_f \delta_{i,j} + \sum_{\nu=1}^4 \frac{\eta_{i,\nu}}{2} \left[e^{ia\mu_{f,I} \delta_{\nu,4}} U_{i;\nu}^{(2)} \delta_{i,j-\hat{\nu}} \right. \\
 &\quad \left. - e^{-ia\mu_{f,I} \delta_{\nu,4}} U_{i-\hat{\nu};\nu}^{(2)\dagger} \delta_{i,j+\hat{\nu}} \right]. \quad (4)
 \end{aligned}$$

The gauge link variables U are used to construct the tree level improved Symanzik pure gauge action [41, 42], S_{YM} , where $W_{i; \mu\nu}^{n \times m}$ is the trace of the $n \times m$ rectangular loop constructed along the directions μ, ν departing from the i site. The staggered Dirac operator $(M_{\text{st}}^f)_{i,j}$, instead, is built up in terms of the two times stout-smearred [43] links $U_{i;\nu}^{(2)}$, in order to reduce taste symmetry violations,

with an isotropic smearing parameter $\rho = 0.15$. As usual, the rooting procedure is adopted to remove the residual degeneracy of the staggered Dirac operator.

When thermal boundary conditions (periodic/anti-periodic for boson/fermion fields) are taken in the temporal direction, the temperature of the system is given by $T = 1/(N_t a)$, where N_t is the number of temporal lattice sites and a is the lattice spacing, related to the bare parameters of the theory. For a given number of lattice sites in the temporal direction, we can choose the simulated temperature by tuning the value of the bare coupling constant β and the quark masses m_s and $m_u = m_d \equiv m_l$, in order to change the lattice spacing while remaining on a line of constant physics, where $m_\pi \simeq 135$ MeV and $m_s/m_l = 28.15$; this line has been determined by a spline interpolation of the results reported in Refs. [44–46].

Let us now sketch the structure of the phase diagram at imaginary μ_B . This has already been done in the introduction, by considering the effective degrees of freedom at work in the different regimes; now we will proceed through an analysis of the properties of the path integral. In the presence of a purely baryonic chemical potential (i.e. $\mu_Q = 0$ and $\mu_S = 0$), one has $\mu_u = \mu_d = \mu_s \equiv \mu_q = \mu_B/3$. When μ_q is purely imaginary, its introduction is equivalent to a global rotation of fermionic boundary conditions in the temporal direction by an angle $\theta_q = \text{Im}(\mu_q)/T$, therefore one expects at least a 2π -periodicity in θ_q ($2\pi N_c$ in θ_B). However, the actual periodicity is $2\pi/N_c$, since a rotation of the fermionic boundary conditions by that angle is equivalent to a center transformation on the gauge fields, hence it can be reabsorbed without modifying the path integral [10].

Numerical simulations show that such a periodicity is smoothly realized at low temperatures [8, 9]. At high T , instead, since the Polyakov loop L (trace of the temporal Wilson line normalized by N_c) enters the fermionic determinant expansion multiplied by $\exp(i\theta_q)$, the value of θ_q selects the true vacuum among the three different minima of the Polyakov loop effective potential, which are related to each other by center transformations. Hence, phase transitions occur as θ_q crosses the boundary between two different center sectors, i.e. for $\theta_q = (2k+1)\pi/N_c$ and k integer (in which case θ_B is an odd multiple of π), where $\langle L \rangle$ jumps from one center sector to the other [10]; the phase of L can serve as a possible order parameter in this case. The T - θ_q phase diagram then consists of a periodic repetition of first order lines (RW lines) in the high- T regime, which disappear at low T . Therefore they have an endpoint at some temperature T_{RW} , where an exact Z_2 symmetry breaks spontaneously. A schematic view of the diagram is reported in Fig. 1.

An alternative order parameter is represented by any of the quark number densities (where $q = u, d, s$)

$$\langle n_q \rangle \equiv \frac{1}{V_4} \frac{\partial \log Z}{\partial \mu_q} \quad (5)$$

where V_4 is the four dimensional lattice volume. Since Z

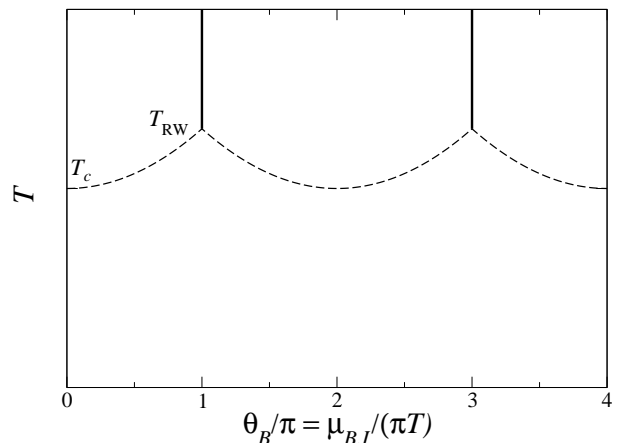


FIG. 1: Phase diagram of QCD in the presence of an imaginary baryon chemical potential. The vertical lines represent the Roberge-Weiss transitions taking place in the high- T regime, while the dashed lines represent the analytic continuation of the pseudocritical line.

is an even function of μ_B , each $\langle n_q \rangle$ is odd and, for purely imaginary μ_B , it is purely imaginary as well. Invariance under charge conjugation, or alternatively oddness and the required 2π periodicity in θ_B , implies that $\langle n_q \rangle$ vanishes for $\theta_B = \pi$ or integer multiples of it, unless a discontinuity takes place at such points, in correspondence of a spontaneous breaking of charge conjugation invariance. This is exactly what happens at the RW lines, so that a non-zero $\langle n_q \rangle$ signals the onset of the RW transition.

In the following, it will be convenient to consider one particular RW line, corresponding to $\theta_q = \pi$, for which the imaginary part of the Polyakov loop, together with the imaginary part of the quark number density, can be taken as an order parameter. The order parameter susceptibility is then defined as

$$\chi_L \equiv N_t N_s^3 (\langle (\text{Im}(L))^2 \rangle - \langle |\text{Im}(L)| \rangle^2), \quad (6)$$

where N_s (N_t) is the spatial (temporal) size in lattice units. The susceptibility χ_L is expected to scale, moving around the endpoint at fixed N_t and θ_q , as

$$\chi_L = N_s^{\gamma/\nu} \phi(t N_s^{1/\nu}), \quad (7)$$

where $t = (T - T_{RW})/T_{RW}$ is the reduced temperature, which is proportional to $(\beta - \beta_{RW})$ close enough to the critical point. That means that the quantity $\chi_L/N_s^{\gamma/\nu}$, measured on different spatial sizes, should lie on the same curve when plotted against $(\beta - \beta_{RW})N_s^{1/\nu}$. Alternatively, we will consider also the susceptibility of the imaginary part of the quark number density, which is defined, for every flavor q , by

$$\chi_q \equiv N_t N_s^3 (\langle [\text{Im}(n_q)]^2 \rangle - \langle |\text{Im}(n_q)| \rangle^2), \quad (8)$$

and is expected to show a scaling behavior as in Eq. (7).

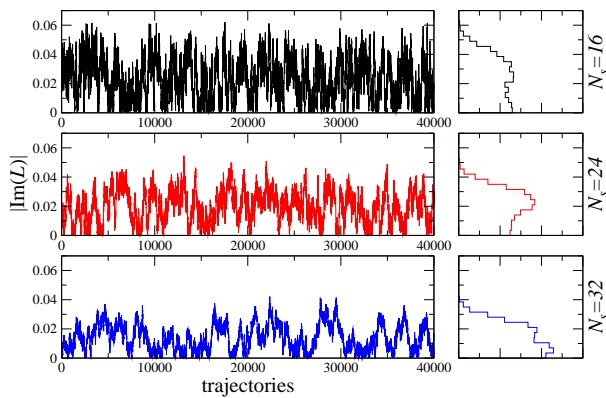


FIG. 2: Monte Carlo histories of $|\text{Im}L|$ for $N_t = 4$ and the β values closest to the peak of χ_L , showing the peculiar features expected near a second order transition: the increase of the autocorrelation time and the absence of a double peak structure in the histogram.

III. NUMERICAL RESULTS

In this Section we present our numerical results, starting from an analysis of the critical behavior around the RW endpoint transition, in order to assess its order and universality class on lattices with $N_t = 4, 6$. Then we will consider also lattices with $N_t = 8, 10$ in order to provide a continuum extrapolated value for T_{RW} .

Since we are interested in studying the behavior near the phase transition, long time histories are required, to cope with the critical slowing down (see Fig. 2); for the couplings around the critical value, we used $\sim 40 - 50K$ trajectories for each run when performing the finite size analysis.

A. Finite size scaling and universality class of the transition

The effective theory associated with the spontaneous breaking of the charge conjugation at finite temperature is a three dimensional theory with Z_2 symmetry, so the transition can be either first order or second order in the three-dimensional Ising universality class. A tricritical scaling is in principle possible as well; however the tricritical point is just a single point at the boundary of first and second order regions. As a consequence (apart from the unlikely case of being exactly on it) tricritical indices can be observed only as scaling corrections, the ultimate large volume behavior being either first order or Ising $3d$ [15, 47–49]. The critical indices that will be used in the following are reported for convenience in Table I.

We will now present the finite size scaling analysis performed to identify the nature of the transition on lattices with temporal extent $N_t = 4$ and 6. As previously discussed, we adopt two different order parameters, namely the imaginary part of the average Polyakov loop and the quark number density; the former turned out to have

	ν	γ	γ/ν	$1/\nu$
3D Ising	0.6301(4)	1.2372(5)	~ 1.963	~ 1.587
1 st Order	1/3	1	3	3

TABLE I: The critical exponents relevant for this study (see e.g. [50, 51]).

smaller correction to scaling, so we will start our analysis from the study of the susceptibility χ_L defined in Eq. (6).

Fig. 3 shows χ_L obtained on $N_t = 4$ lattices and rescaled according to Eq. (7), using alternatively the critical indices of the $3d$ Ising universality class or those corresponding to a first order transition (the values used for the critical coupling are the ones reported in Table II). Using $3d$ Ising indices the results on different volumes collapse on top of each other, whereas this is not the case using first order indices, which strongly indicates that the transition is second order for $N_t = 4$. Note that, since we are performing simulations on a line of constant physics, the mass parameters change with β ; it is thus not possible to use standard reweighting methods [52, 53]. In Fig. 4 we repeat the same analysis using the Polyakov loop measured on lattices with temporal extent $N_t = 6$. Again, the $3d$ -Ising universality class appears to describe the scaling of the susceptibility of the Polyakov loop significantly better than a first order, although larger corrections to scaling are present with respect to the $N_t = 4$ case.

A confirmation of the previous analysis comes from the study of the fourth-order Binder ratio, which in our case is defined as

$$B_4 = \frac{\langle (\text{Im}L)^4 \rangle}{\langle (\text{Im}L)^2 \rangle^2}. \quad (9)$$

It is easy to show that, in the thermodynamical limit, $B_4 \rightarrow 3$ in the absence of a phase transition, while $B_4 \rightarrow 1$ if a first order transition is present. At second order transitions B_4 assumes non-trivial values, which are characteristic of the universal critical behavior associated with the transition [50, 54, 55]. For the particular case of the three-dimensional Ising universality class the critical value is $B_4 = 1.604(1)$, see Ref. [51]. From these general properties the following simple procedure follows to locate the critical endpoint of a line of first order transition: study the behavior of B_4 as a function of the coupling for different values of the lattice size; the endpoint coupling value will correspond (up to scaling corrections) to the crossing point of these curves.

In Fig. 5 we show the values of B_4 in a neighborhood of the critical coupling at three different volumes both on $N_t = 4$ and $N_t = 6$ temporal extent. The behavior of the Binder ratio as a function of β is clearly the one expected at a critical endpoint and the value at the crossing point is in reasonable agreement with that expected for a transition of the $3d$ Ising universality class, while a first order is clearly excluded.

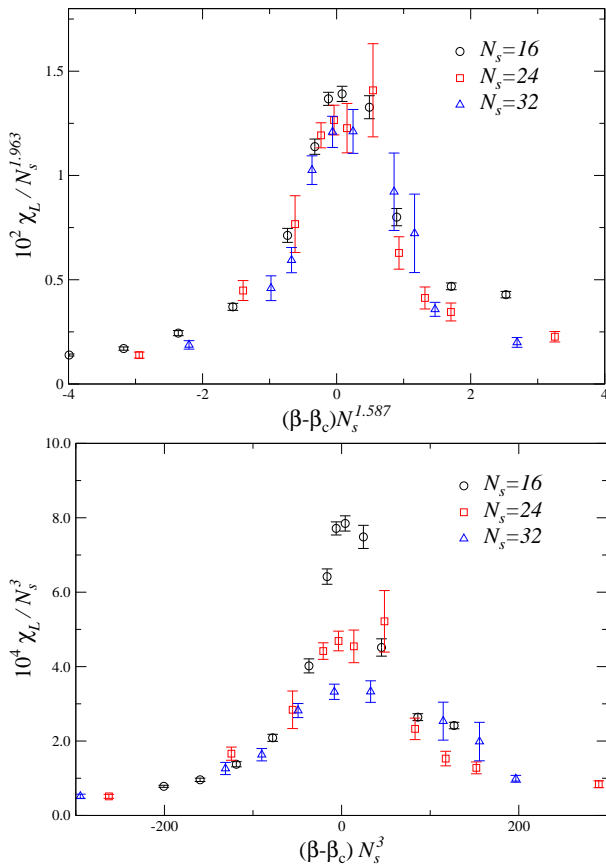


FIG. 3: Susceptibility of the imaginary part of the Polyakov loop on $N_t = 4$ lattices rescaled using the 3d Ising critical indices (top) or the first order ones (bottom).

The same conclusions are obtained by studying the susceptibility of the u quark number density defined in Eq. (8), although in this case the scaling corrections appear to be larger. As an example in Fig. 6 we show the behavior of χ_u on $N_t = 4$ lattices, rescaled according to Eq. (7): again, the 3d-Ising critical indices are favored. The case of the strange susceptibility χ_s is similar, as well as the $N_t = 6$ case.

B. Critical temperature: continuum extrapolated value

Having established that the RW-transition is second order for lattices with temporal extent $N_t = 4$ and 6, we now proceed to estimate the continuum value of T_{RW} . To this purpose, simulations have been performed also on lattices with $N_t = 8$ and 10, considering a limited number of spatial volumes (one or two) per simulation setup.

The pseudocritical value of the coupling has been determined for each lattice size by estimating the position of the maximum of χ_L and χ_u . To this purpose, we have

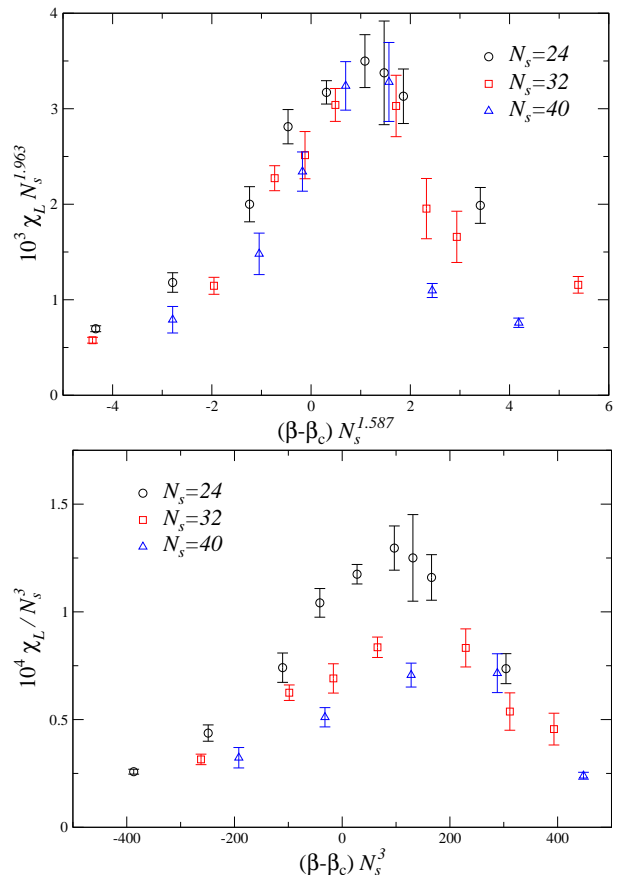


FIG. 4: Susceptibility of the imaginary part of the Polyakov loop on $N_t = 6$ lattices rescaled using the 3d Ising critical indices (top) or the first order ones (bottom).

fitted the peak with a Lorentzian function:

$$f(\beta) = \frac{a}{1 + (\beta - \beta_{pc})^2 / c^2}. \quad (10)$$

The results for the large volume limit of β_{pc} , denoted by β_c , are reported in Table II; the error also takes into account the systematics related to the choice of the fit range. The volume dependence of the pseudocritical coupling is very mild for lattice with aspect ratio 4 or larger, with variations at the level of 0.1% in terms of β (which become 0.5% in terms of temperature), as can be seen in Fig. 7 for the case of the $N_t = 4$ lattices. The pseudocritical couplings determined by using χ_L or χ_u have *a priori* to coincide only in the thermodynamical limit, however in all the cases the differences between the two determinations are well below 0.1% and, with the exception of the lattice 4×16^3 , they are compatible with each other at one standard deviation.

In order to convert the critical temperatures to physical units we used the lattice spacings values reported in Tab. II, which are obtained by a spline interpolation of the results presented in [44–46]. The systematic uncertainty on these lattice spacings is 2–3% [44–46] and this is by far the largest source of error in the final tempera-

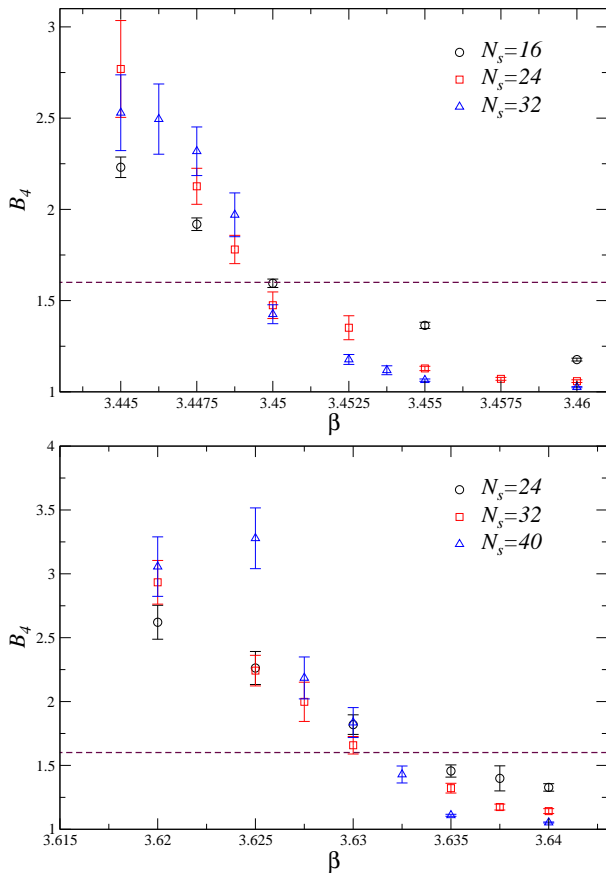


FIG. 5: Binder fourth order ratio of the Polyakov loop imaginary part computed on $N_t = 4$ lattices (top) and $N_t = 6$ lattices (bottom). The horizontal line denotes the value expected for a second order transition of the 3d Ising universality class.

N_t	β_c	N_s	a (fm)
4	3.4498(7)	16, 24, 32	0.2424(6)
6	3.6310(15)	24, 32, 40	0.1714(3)
8	3.7540(25)	32, 40	0.1233(3)
10	3.8600(25)	40	0.0968(2)

TABLE II: Critical values of the coupling for different N_t values (estimated by using lattices of spatial extent N_s) and corresponding values for the lattice spacing. Only the statistical error of the lattice spacing is reported in the table, the systematic error is about 2 – 3% [44–46].

ture estimates. The results obtained at the different N_t are plotted in Fig. 8 together with the linear fit in $1/N_t^2$, which describes well the approach to the continuum limit and from which we extract the value 208(4) MeV for the continuum limit of the RW endpoint temperature. Using as systematical error the difference between this value and the one obtained using just the three finer lattices, we get our final estimate $T_{\text{RW}} = 208(5)$ MeV.

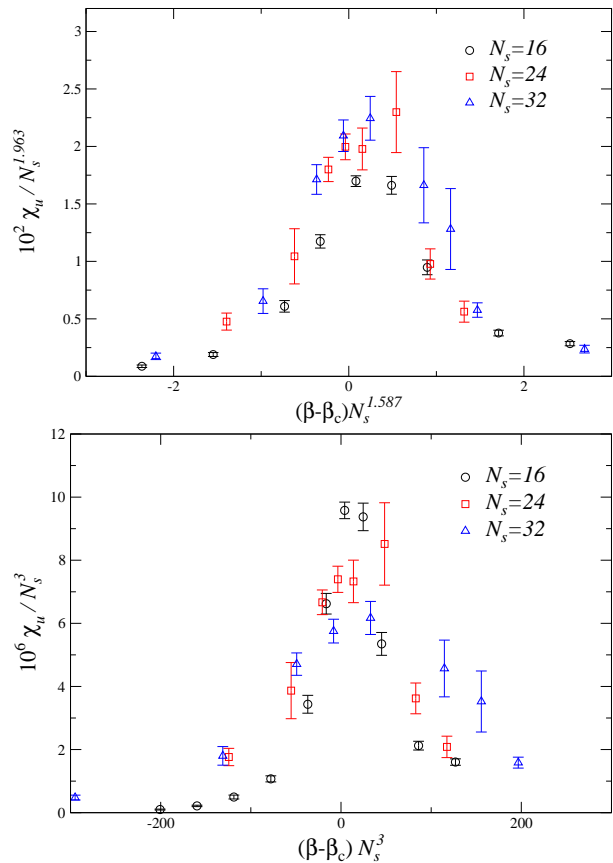


FIG. 6: Disconnected susceptibility of the light baryon number computed on $N_t = 4$ lattices and rescaled with the critical exponents of the 3d Ising universality class (top) or corresponding to a first order transition (bottom).

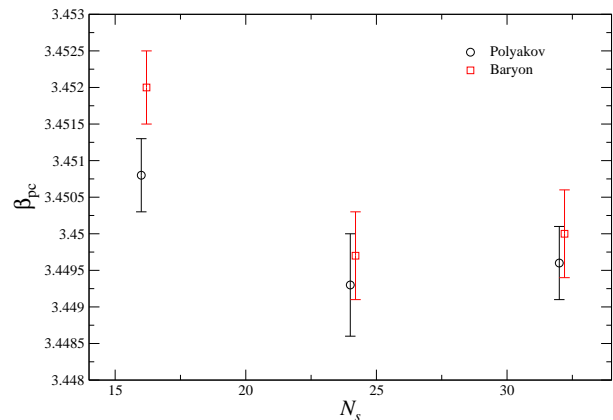


FIG. 7: Thermodynamical limit of the pseudocritical coupling determined on $N_t = 4$ lattices from the maxima of χ_L and χ_B .

C. Relation with the pseudocritical chiral transition line

An interesting issue that remains to be investigated is the relation between the RW endpoint and the chiral

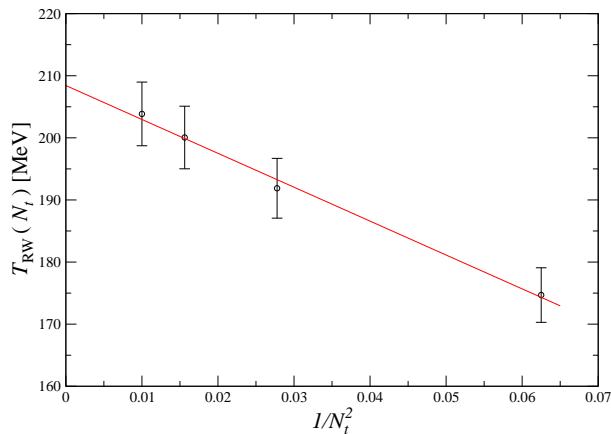


FIG. 8: Continuum extrapolation of the critical temperature.

transition. In particular, the question can be posed in the following way: does the pseudocritical line really get to the RW endpoint, as assumed in Fig. 1 and as suggested by early studies on the subject?

A number of investigations appeared recently, reproducing the pseudocritical line for imaginary chemical potentials at or close to the physical point and with the setup of chemical potentials relevant to the RW endpoint, i.e. $\mu_s = \mu_l = \mu_B/3$, see Refs. [56–59]. A possible way to approach the question is to try extrapolating the location of the pseudocritical line up to $\theta_B = \pi$ on the basis of those determinations. To this aim we considered results for $T_c(\theta_B)$ obtained in Ref. [58] on $N_t = 8$ lattices and adopting the same discretization used in the present study. In Fig. 9, we present two different extrapolations of such data, corresponding to the fit ansatz

$$T_c(\theta_B) = T_c(1 + \kappa \theta_B^2 + b \theta_B^4 + c \theta_B^6) \quad (11)$$

with or without the sixth order term included (a simple linear dependence on θ_B^2 was excluded in Ref. [58]). In both cases one gets reasonably close, within errors, to the RW endpoint.

Of course, the issue can be checked also directly, by determining the location of the pseudocritical line exactly at $\theta_B = \pi$. To that aim, in Fig. 10 we plot the renormalized light chiral susceptibility (as defined, e.g., in Ref. [58]) for lattices with temporal extent $N_t = 6, 8$, together with the positions of the RW endpoint as previously determined on the same lattices. It is clearly seen that the location of the maxima of the chiral susceptibility is compatible with the position of the RW endpoints. For instance for $N_t = 8$ and $N_s = 32$ we obtain, by fitting the chiral susceptibility to a Lorentzian peak, $\beta_c = 3.749(3)$, which is at just one standard deviation from the RW endpoint coupling reported in Table II.

We can thus confirm, within present errors, evidence that the RW endpoint is located at a point where the analytic continuation of the pseudocritical line and the RW first order line meet each other. To conclude, based on this evidence, we have performed a final fit, including

terms up to the sixth order in θ_B^2 , which includes the RW endpoint as a part of the pseudocritical line. The result is the dashed line reported in Fig. 9, which has been continued also to the other center sectors, so as to reproduce a realistic version (i.e. for $N_f = 2 + 1$ QCD with physical quark masses, even if just for $N_t = 8$) of the phase diagram sketched in Fig. 1.

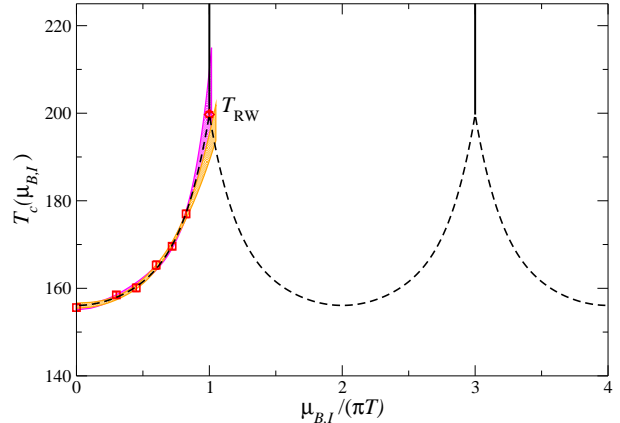


FIG. 9: Phase diagram of QCD in the presence of an imaginary baryon chemical potential obtained from numerical simulations on $N_t = 8$ lattices alone. Bands denote fits to polynomials in μ_B^2 : the orange (longer) band is obtained using terms up to order μ_B^4 , the violet (shorter) one using up to μ_B^6 terms.

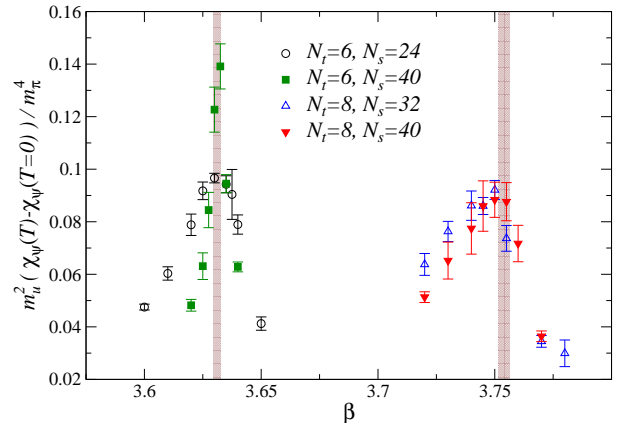


FIG. 10: Renormalized light chiral susceptibility on $N_t = 6$ and 8 lattices. The vertical bands denote the position of the RW endpoint on lattices of the corresponding temporal extent.

IV. CONCLUSIONS

We have investigated the properties of the RW endpoint by lattice simulations of $N_f = 2 + 1$ QCD with physical quark masses and making use of two different order parameters for the transition, namely the imaginary part of the Polyakov line and the imaginary part of

the quark number density, which have led to consistent results.

The temperature of the endpoint, T_{RW} , has been determined at four different values of the lattice temporal extent, $N_t = 4, 6, 8, 10$, from which we have obtained a continuum extrapolated value $T_{RW} = 208(5)$ MeV, where the error includes both statistical and systematic contributions, stemming mostly from the determination of the physical scale. That leads to the estimate $T_{RW}/T_c = 1.34(7)$, where the error also takes into account the systematics involved in the determination of T_c , originating both from the scale setting and from the difficulties in defining a critical temperature when no real transition is present. This ratio is significantly larger than the ones obtained in previous studies; indeed, with unimproved actions, unphysical quark masses and no extrapolation to the continuum limit, T_{RW} was typically found to be only about 10% larger than T_c . The larger value is partially due to the larger curvature κ , and partially to the more significant contribution from non-linear terms in μ_B^2 (see Eq. (11)) which are present in the case $\mu_u = \mu_d = \mu_s$ (see Ref. [58]).

Regarding the order of the transition, our finite size scaling analysis provides evidence that a second order transition of the 3d-Ising universality class takes place, rather than a first order one, at least for $N_t = 4$ and $N_t = 6$ lattices. Our investigation has been performed at a fixed value of the pion mass, corresponding to its physical value $m_\pi \simeq 135$ MeV.

Previous studies on the subject, performed in the $N_f = 2$ theory with both staggered and Wilson fermions, have shown that the order of the transition changes as a function of m_π ; in particular, there are two tricritical pion masses, $m_\pi^{\text{tric.light}}$ and $m_\pi^{\text{tric.heavy}}$, and the transition is second order for $m_\pi^{\text{tric.light}} < m_\pi < m_\pi^{\text{tric.heavy}}$ and first order for lighter or heavier pion masses. The value of the heavy tricritical mass is typically well above the GeV scale. The lighter critical pion mass has been found to be $m_\pi^{\text{tric.light}} \sim 400$ MeV for standard staggered fermions on $N_t = 4$ lattices [15], and around 930 and 680 MeV for standard Wilson fermions on respectively $N_t = 4$ [19] and $N_t = 6$ [25] lattices. Given these results, even if we have studied just the physical value of the pion mass, we can conclude the following: for stout improved staggered fermions, one has $m_\pi^{\text{tric.light}} < 135$ MeV on both the $N_t = 4$ and $N_t = 6$ lattices. When compared to previous results, that demonstrates the presence of significant cut-off effects on the values of this tricritical mass, even when working at fixed N_t but with a different action. Moreover, based on the observed tendency of the tricritical mass to decrease with the increase of N_t , we suggest that $m_\pi^{\text{tric.light}}$ should be smaller than $m_\pi^{\text{phys}} = 135$ MeV in the continuum limit, so that the RW endpoint should be a second order transition in the continuum limit at the physical pion mass.

We must however remark that the mechanism driving the change of nature of RW endpoint transition, from second to first order as the pion mass decreases, is still

unknown. If such a mechanism is related to the chiral properties of quarks, unexpected behaviors could occur as the continuum chiral symmetry group is fully recovered. This is known to happen, at least for staggered fermions, for lattice spacings well below those explored in the present study (see Ref. [60] for a recent investigation about this issue).

Let us spend a few words about what, in our opinion, future studies should clarify. First of all, one would like to check the second order nature of the RW endpoint at the physical point on finer lattices, i.e. for $N_t > 6$. Then, our study with stout improved staggered fermions should be extended to different values of the pion mass, in order to locate the values of the tricritical masses $m_\pi^{\text{tric.light}}$ and $m_\pi^{\text{tric.heavy}}$ and possibly extrapolate them to the continuum limit. Such a program, which goes beyond our present computational capabilities, would clarify the universal properties of the only critical point of strong interactions (in the presence of finite quark masses) that one can predict *a priori*, based on the known symmetries of QCD.

Finally, another open issue regards the relation of the RW critical point to those predicted in well defined limits of QCD. The relation to the deconfinement transition present in the quenched case is obvious, since the two transitions trivially coincide in this case and are both related to center symmetry. The relation to the chiral transition in the limit of massless quarks is far less trivial. Suppose to move (varying the temperature) along the line $\theta_B = \pi$ in the presence of massless quarks; in principle one expects two different critical temperatures, one at which chiral symmetry is restored, T_χ , and one at which the Z_2 charge conjugation symmetry spontaneously breaks, T_{RW} . What is the relation between T_χ and T_{RW} ? Our present results at finite quark masses prove that the location of the peak of the renormalized chiral susceptibility coincides, within errors, with T_{RW} , see Fig. 10, so that the analytic continuation of the pseudocritical line meets the RW line at its endpoint. However, in order to obtain a definite answer, the issue should be explored while approaching the chiral limit: this is something which goes beyond the purpose of the present study and is left to future investigations.

Acknowledgments

It is a pleasure to thank P. de Forcrand for very useful comments. Numerical simulations have been performed on the BlueGene/Q Fermi machine at CINECA, based on the Project Iskra-B/CRIBEQCD and on the agreement between INFN and CINECA (under project INF14_npqcd), and on the CSN4 Zefiro cluster of the Scientific Computing Center at INFN-PISA. FN acknowledges financial support from the INFN SUMA project. FS received funding from the European Research Council under the European Community Seventh Framework Programme (FP7/2007-2013) ERC grant agreement No

-
- [1] Y. Aoki, G. Endrodi, Z. Fodor, S. D. Katz and K. K. Szabo, *Nature* **443** (2006) 675 [hep-lat/0611014].
- [2] Y. Aoki, Z. Fodor, S. D. Katz and K. K. Szabo, *Phys. Lett. B* **643**, 46 (2006) [hep-lat/0609068].
- [3] S. Borsanyi *et al.* [Wuppertal-Budapest Collaboration], *JHEP* **1009**, 073 (2010) [arXiv:1005.3508 [hep-lat]].
- [4] A. Bazavov, T. Bhattacharya, M. Cheng, C. DeTar, H. T. Ding, S. Gottlieb, R. Gupta and P. Hegde *et al.*, *Phys. Rev. D* **85**, 054503 (2012) [arXiv:1111.1710 [hep-lat]].
- [5] T. Bhattacharya *et al.*, *Phys. Rev. Lett.* **113**, no. 8, 082001 (2014) [arXiv:1402.5175 [hep-lat]].
- [6] M. G. Alford, A. Kapustin, and F. Wilczek, *Phys. Rev. D* **59**, 054502 (1999) [hep-lat/9807039].
- [7] M.-P. Lombardo, *Nucl. Phys. Proc. Suppl.* **83**, 375 (2000) [hep-lat/9908006].
- [8] P. de Forcrand and O. Philipsen, *Nucl. Phys. B* **642**, 290 (2002) [hep-lat/0205016]; *Nucl. Phys. B* **673**, 170 (2003) [hep-lat/0307020].
- [9] M. D’Elia and M. P. Lombardo, *Phys. Rev. D* **67**, 014505 (2003) [hep-lat/0209146]; *Phys. Rev. D* **70**, 074509 (2004) [hep-lat/0406012].
- [10] A. Roberge and N. Weiss, *Nucl. Phys. B* **275**, 734 (1986).
- [11] M. D’Elia, F. Di Renzo and M. P. Lombardo, *Phys. Rev. D* **76**, 114509 (2007) [arXiv:0705.3814 [hep-lat]].
- [12] P. Cea, L. Cosmai, M. D’Elia, C. Manneschi and A. Papa, *Phys. Rev. D* **80**, 034501 (2009) [arXiv:0905.1292 [hep-lat]].
- [13] M. D’Elia and F. Sanfilippo, *Phys. Rev. D* **80**, 111501 (2009) [arXiv:0909.0254 [hep-lat]].
- [14] P. de Forcrand and O. Philipsen, *Phys. Rev. Lett.* **105**, 152001 (2010) [arXiv:1004.3144 [hep-lat]].
- [15] C. Bonati, G. Cossu, M. D’Elia and F. Sanfilippo, *Phys. Rev. D* **83**, 054505 (2011) [arXiv:1011.4515 [hep-lat]].
- [16] P. Cea, L. Cosmai, M. D’Elia, A. Papa and F. Sanfilippo, *Phys. Rev. D* **85**, 094512 (2012) [arXiv:1202.5700 [hep-lat]].
- [17] A. Alexandru and A. Li, *PoS LATTICE 2013*, 208 (2013) [arXiv:1312.1201 [hep-lat]].
- [18] L.-K. Wu and X.-F. Meng, *Phys. Rev. D* **87**, 094508 (2013) [arXiv:1303.0336 [hep-lat]].
- [19] O. Philipsen and C. Pinke, *Phys. Rev. D* **89**, 094504 (2014) [arXiv:1402.0838 [hep-lat]].
- [20] L.-K. Wu and X.-F. Meng, *Phys. Rev. D* **90**, 094506 (2014) [arXiv:1405.2425 [hep-lat]].
- [21] C. Bonati, P. de Forcrand, M. D’Elia, O. Philipsen and F. Sanfilippo, *Phys. Rev. D* **90**, 074030 (2014) [arXiv:1408.5086 [hep-lat]].
- [22] K. Nagata, K. Kashiwa, A. Nakamura and S. M. Nishigaki, *Phys. Rev. D* **91**, 094507 (2015) [arXiv:1410.0783 [hep-lat]].
- [23] T. Makiyama *et al.*, *Phys. Rev. D* **93**, 014505 (2016) [arXiv:1502.06191 [hep-lat]].
- [24] C. Pinke and O. Philipsen, arXiv:1508.07725 [hep-lat].
- [25] F. Cuteri, C. Pinke, A. Sciarra, C. Czaban and O. Philipsen, arXiv:1512.07180 [hep-lat].
- [26] T. DeGrand and R. Hoffmann, *JHEP* **0702**, 022 (2007) [hep-lat/0612012].
- [27] B. Lucini, A. Patella and C. Pica, *Phys. Rev. D* **75**, 121701 (2007) [hep-th/0702167].
- [28] H. Kouno, Y. Sakai, K. Kashiwa and M. Yahiro, *J. Phys. G* **36**, 115010 (2009) [arXiv:0904.0925 [hep-ph]].
- [29] Y. Sakai, K. Kashiwa, H. Kouno, M. Matsuzaki and M. Yahiro, *Phys. Rev. D* **79**, 096001 (2009) [arXiv:0902.0487 [hep-ph]].
- [30] Y. Sakai, T. Sasaki, H. Kouno and M. Yahiro, *Phys. Rev. D* **82**, 076003 (2010) [arXiv:1006.3648 [hep-ph]].
- [31] T. Sasaki, Y. Sakai, H. Kouno and M. Yahiro, *Phys. Rev. D* **84**, 091901 (2011) [arXiv:1105.3959 [hep-ph]].
- [32] H. Kouno, M. Kishikawa, T. Sasaki, Y. Sakai and M. Yahiro, *Phys. Rev. D* **85**, 016001 (2012) [arXiv:1110.5187 [hep-ph]].
- [33] G. Aarts, S. P. Kumar and J. Rafferty, *JHEP* **1007**, 056 (2010) [arXiv:1005.2947 [hep-th]].
- [34] J. Rafferty, *JHEP* **1109**, 087 (2011) [arXiv:1103.2315 [hep-th]].
- [35] K. Morita, V. Skokov, B. Friman and K. Redlich, *Phys. Rev. D* **84**, 076009 (2011) [arXiv:1107.2273 [hep-ph]].
- [36] K. Kashiwa, T. Hell and W. Weise, *Phys. Rev. D* **84**, 056010 (2011) [arXiv:1106.5025 [hep-ph]].
- [37] V. Pagura, D. Gomez Dumm and N. N. Scoccola, *Phys. Lett. B* **707**, 76 (2012) [arXiv:1105.1739 [hep-ph]].
- [38] D. Scheffler, M. Buballa and J. Wambach, *Acta Phys. Polon. Supp.* **5**, 971 (2012) [arXiv:1111.3839 [hep-ph]].
- [39] K. Kashiwa and R. D. Pisarski, *Phys. Rev. D* **87**, 096009 (2013) [arXiv:1301.5344 [hep-ph]].
- [40] K. Kashiwa, T. Sasaki, H. Kouno and M. Yahiro, *Phys. Rev. D* **87**, 016015 (2013) [arXiv:1208.2283 [hep-ph]].
- [41] P. Weisz, *Nucl. Phys. B* **212**, 1 (1983).
- [42] G. Curci, P. Menotti and G. Paffuti, *Phys. Lett. B* **130**, 205 (1983) [Erratum-ibid. *B* **135**, 516 (1984)].
- [43] C. Morningstar and M. J. Peardon, *Phys. Rev. D* **69**, 054501 (2004) [hep-lat/0311018].
- [44] Y. Aoki, S. Borsanyi, S. Durr, Z. Fodor, S. D. Katz, S. Krieg and K. K. Szabo, *JHEP* **0906**, 088 (2009) [arXiv:0903.4155 [hep-lat]].
- [45] S. Borsanyi, G. Endrodi, Z. Fodor, A. Jakovac, S. D. Katz, S. Krieg, C. Ratti and K. K. Szabo, *JHEP* **1011**, 077 (2010) [arXiv:1007.2580 [hep-lat]].
- [46] S. Borsanyi, Z. Fodor, C. Hoelbling, S. D. Katz, S. Krieg and K. K. Szabo, *Phys. Lett. B* **730**, 99 (2014) [arXiv:1309.5258 [hep-lat]].
- [47] C. Bonati and M. D’Elia, *Phys. Rev. D* **82**, 114515 (2010). [arXiv:1010.3639 [hep-lat]].
- [48] C. Bonati and M. D’Elia, *Phys. Rev. D* **88**, no. 6, 065025 (2013). [arXiv:1305.3564 [hep-lat]].
- [49] I. D. Lawrie and S. Sarbach, *Theory of Tricritical Points*, in C. Domb, J. L. Lebowitz (eds.) “Phase transitions and critical phenomena, vol. 11”, Academic Press (1987).
- [50] A. Pelissetto and E. Vicari, *Phys. Rep.* **368**, 549 (2002) [arXiv:cond-mat/0012164].
- [51] H. W. J. Blöte, E. Luijten and J. R. Heringa, *J. Phys. A: Math. Gen.* **28** 6289 (1995) [arXiv:cond-mat/9509016].
- [52] A. M. Ferrenberg and R. H. Swendsen *Phys. Rev. Lett.* **61**, 2635 (1988).
- [53] A. M. Ferrenberg and R. H. Swendsen *Phys. Rev. Lett.*

- 63**, 1195 (1989).
- [54] K. Binder, Phys. Rev. Lett. **47**, 693 (1981).
- [55] K. Binder, Z. Phys. B - Condensed Matter **43**, 119 (1981).
- [56] P. Cea, L. Cosmai and A. Papa, Phys. Rev. D **89**, 074512 (2014) [arXiv:1403.0821 [hep-lat]].
- [57] C. Bonati, M. D'Elia, M. Mariti, M. Mesiti, F. Negro and F. Sanfilippo, Phys. Rev. D **90**, 114025 (2014) [arXiv:1410.5758 [hep-lat]].
- [58] C. Bonati, M. D'Elia, M. Mariti, M. Mesiti, F. Negro and F. Sanfilippo, Phys. Rev. D **92**, 054503 (2015) [arXiv:1507.03571 [hep-lat]].
- [59] P. Cea, L. Cosmai and A. Papa, Phys. Rev. D **93**, 014507 (2016) [arXiv:1508.07599 [hep-lat]].
- [60] C. Bonati, M. D'Elia, M. Mariti, G. Martinelli, M. Mesiti, F. Negro, F. Sanfilippo and G. Villadoro, JHEP **1603**, 155 (2016) [arXiv:1512.06746 [hep-lat]].